

Janus and Huygens Dipoles: Near-Field Directionality Beyond Spin-Momentum Locking

Michela F. Picardi,^{*} Anatoly V. Zayats, and Francisco J. Rodríguez-Fortuño

Department of Physics, King's College London, Strand, London, WC2R 2LS, United Kingdom



(Received 27 October 2017; published 15 March 2018)

Unidirectional scattering from circularly polarized dipoles has been demonstrated in near-field optics, where the quantum spin-Hall effect of light translates into spin-momentum locking. By considering the whole electromagnetic field, instead of its spin component alone, near-field directionality can be achieved beyond spin-momentum locking. This unveils the existence of the Janus dipole, with side-dependent topologically protected coupling to waveguides, and reveals the near-field directionality of Huygens dipoles, generalizing Kerker's condition. Circular dipoles, together with Huygens and Janus sources, form the complete set of all possible directional dipolar sources in the far- and near-field. This allows the designing of directional emission, scattering, and waveguiding, fundamental for quantum optical technology, integrated nanophotonics, and new metasurface designs.

DOI: [10.1103/PhysRevLett.120.117402](https://doi.org/10.1103/PhysRevLett.120.117402)

Nanoscale emitters, scatterers, and their assemblies have been recently considered for quantum optical technologies, metasurface designs enabling flat lenses, holograms, and scalable photonic circuitry, where the requirements on miniaturization and efficient coupling to photonic modes are strict [1–3]. Scatterers can be realized as strongly resonant plasmonic or high-index dielectric nanoparticles supporting electric and/or magnetic dipolar resonances, while emitters can be quantum dots or atoms. Near field interference and related directional excitation of fields from circularly polarized electric and magnetic dipoles [4–13] have proven to have fascinating applications in quantum optics [14–16] and in novel experimental nanophotonic devices, such as nanorouters, polarimeters, and nonreciprocal optical components [17–25]. These effects rely on the photonic quantum spin-Hall effect exploiting the phenomenon of spin-momentum locking in evanescent and guided waves [26–31]; in essence, the spin of the dipole can be matched to the inherent spin of confined fields to be directionally excited. Electromagnetic spin accounts for the rotation of the electric \mathbf{E} and magnetic \mathbf{H} field vectors; however, it does not account for the relative amplitude and phases *between* electric and magnetic components. By engineering superpositions of electric and magnetic dipoles and their interference [32–35] we can exploit these relations to achieve near-field directionality beyond spin-momentum locking.

An example of a well-known dipolar source that exploits these relations to achieve *far-field* directionality is the Huygens antenna. This source combines two orthogonal linearly polarized electric p and magnetic m dipoles satisfying Kerker's condition [36,37]:

$$p = \frac{m}{c}, \quad (1)$$

with c being the speed of light. Its radiation diagram is highly directional and has zero backscattering, due to the interference of magnetic and electric dipole radiation. These antennas are attracting great attention due to the feasibility of implementing them using high-index dielectric nanoparticles [38–41], with applications in null backscattering metasurfaces, and all-dielectric mirrors [42–48].

Here we show that Huygens sources can be generalized to achieve near-field directionality, and that there exists a dipolar source complementary to a Huygen's dipole, which we term a Janus dipole, with a different relation between the phases of electric and magnetic dipoles, which is not directional in the far-field, but has unique near-field properties allowing side-dependent coupling to guided modes. Together, Huygens, Janus, and circular electric and magnetic dipoles (as well as the infinite spectrum of their linear combinations) provide a general closed solution to dipolar far- and near-field directionality that takes into account the topology of the vector structure of free-space and guided electromagnetic fields. These dipolar sources can be experimentally realized as plasmonic, dielectric, and hybrid nanoparticles.

We consider three elemental dipole sources for near-field directionality: circularly polarized dipoles have spinning electric or magnetic dipole moments, while Huygens and Janus sources combine orthogonal electric and magnetic dipoles that are in phase or 90° out of phase to each other, respectively. Each can be introduced from their close relation to well-known electromagnetic quantities (Fig. 1). First, Huygens sources are often explained in terms of the time-averaged Poynting vector $\propto \text{Re}[\mathbf{E}^* \times \mathbf{H}]$. This vector represents intensity and direction of the electromagnetic power flow. It arises wherever electric and magnetic field are in phase and orthogonal to each other. It follows that, when electric and magnetic dipoles

are orthogonal and in phase—a Huygens source—they produce fields associated with a net power flow in a given direction. This gives rise to directionality in the far field [42–48], but we can exploit the same idea in the near field of a waveguide (Fig. 1). Second, circularly polarized dipole directionality can be explained by means of the spin angular momentum [49] $\propto \text{Im}[\mathbf{E}^* \times \mathbf{E}] + \text{Im}[\mathbf{H}^* \times \mathbf{H}]$, which accounts for the rotation of the vectors \mathbf{E} and \mathbf{H} . Owing to the existence of out-of-phase *longitudinal* components of the fields in guided modes, this spin can be transverse to the propagation direction. Circularly polarized dipoles—two orthogonal electric or magnetic dipole moments, 90° out of phase—exploit this well-known transverse spin-momentum locking [6,28–31], exciting the guided mode in one direction only. Finally, we can consider a third quantity $\propto \text{Im}[\mathbf{E}^* \times \mathbf{H}]$. This expression resembles spin angular momentum, but it mixes electric and magnetic components. It arises when \mathbf{E} and \mathbf{H} are orthogonal but 90° out of phase. This phase shift results in harmonic oscillations of the instantaneous power flow, with a zero time-averaged net flow. This is the imaginary part of the complex Poynting vector, and is known as *reactive power*. It points in the direction of evanescent gradient: away from or towards the nearby waveguide, depending on the mode. We thus propose the Janus source, using orthogonal electric and magnetic dipoles with a 90° phase shift to match or oppose this vector, accounting for its two “faces”: one face couples into the mode, while the other is noncoupling. The three vector quantities, each associated with one of the sources, form a triad at each point near a waveguide [31] (Fig. 1).

As a simple example, Fig. 2 shows the fields generated by (a) a circular dipole, (b) a Huygens antenna, and (c),(d) a Janus dipole for its two orientations, all placed over a dielectric slab waveguide. We used a planar slab as an example, but the directionality of the dipoles is universal and completely independent of the waveguide’s nature. The first two sources lead to directional evanescent wave excitation of guided modes. While this is known for circular dipoles [4–13,29,31], Huygens antennas have been extensively studied for their strong directional radiation diagram, but their near-field directionality had not been explored. The direction of excitation of these sources can be switched by flipping the sign of one of their two dipole components, which can be experimentally achieved tuning polarization and wavelength of the light illuminating the nanoparticle, with respect to its electric and magnetic resonances.

The Janus dipole has an intriguing property: by opposing or matching the direction of reactive power, perpendicular to the waveguide, it either shows (c) a complete absence of coupling, not exciting waveguide modes at all, or (d) excitation of the guided mode in both directions. This is determined by which “side” of the dipole is facing the waveguide. Inverting the sign of one component in the

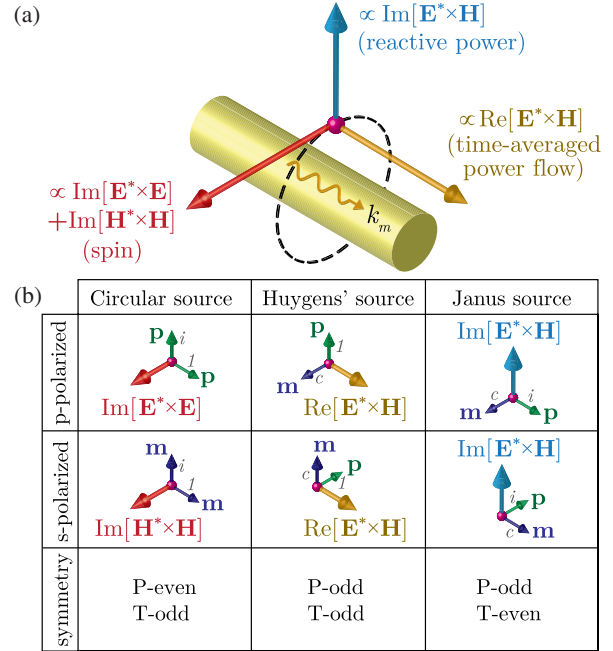


FIG. 1. (a) Triad of vectors (time-averaged power flow, reactive power, and spin vector) associated to any guided mode, each related to one of the three sources in the schematics (b). (b) Schematics of the sources and their relative vectors. The top left panel depicts a circularly polarized electric dipole, superposition of two orthogonal linear electric dipoles \mathbf{p} with complex amplitudes 1 and i , representing their quadrature phase relation. This circular dipole is associated with a transverse spin vector shown in the panel. A similar notation is used throughout the table, using \mathbf{m} for magnetic dipole moments. The spin (red), Poynting (yellow), and reactive power (blue) vectors are associated to different directional dipolar sources, and each of them behaves differently under parity (P) and time-reversal (T) symmetry transformations. Notice that, with respect to time-reversal, \mathbf{E} fields are even while \mathbf{H} fields are odd. Moreover, the operation of taking the real part of respective vectors is time even while taking the imaginary part is time odd.

Janus dipole will change the side facing the waveguide, like when flipping a coin, and this will switch the coupling on and off [Figs. 2(c) and 2(d)]. Alternatively, the dipole’s behavior depends on which side of the waveguide it is placed. Each of these three elemental sources possesses the same symmetries as the vector it is associated with, sharing its behavior under parity (P) and time-reversal (T) symmetry transformations [50], as summarized in Fig. 1(b).

A quantitative explanation of the three sources can be obtained from Fermi’s golden rule [6–9,14,15,31]. This rule dictates that the coupling efficiency between an electric \mathbf{p} and magnetic \mathbf{m} dipole source and a waveguide mode is proportional to $|\mathbf{p} \cdot \mathbf{E}^* + \mathbf{m} \cdot \mu \mathbf{H}^*|^2$, where \mathbf{E} and \mathbf{H} are the electric and magnetic fields, respectively, of the mode calculated at the location of the dipoles, and μ is the permeability of the medium. In Fig. 2, the dipoles are interacting with a p -polarized waveguide mode, so the only

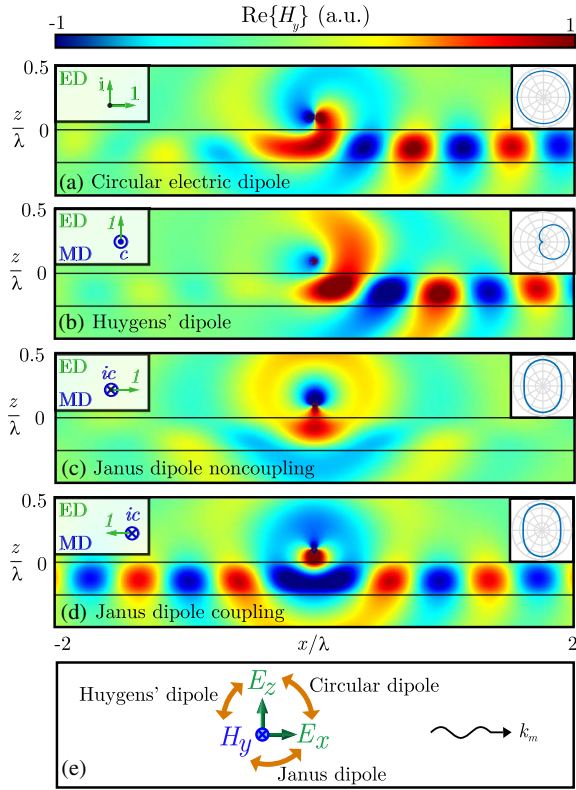


FIG. 2. Magnetic field radiated by (a) a circularly polarized electric dipole $\mathbf{p} = (1, 0, i)$, $\mathbf{m} = (0, 0, 0)$; (b) a Huygens antenna $\mathbf{p} = (0, 0, 1)$, $\mathbf{m} = (0, -c, 0)$; (c),(d) a Janus dipole $\mathbf{p} = (\pm 1, 0, 0)$, $\mathbf{m} = (0, ic, 0)$ in noncoupling (c) and coupling (d) orientation, in close proximity ($z_0 = 0.1\lambda$) to a dielectric slab (index $n = 2$ and thickness $t = \lambda/4$) (e) Schematic of field components excited by each source. The insets show the orientation of the dipoles and the far field radiation diagrams. These fields have been simulated using Comsol Multiphysics.

nonzero field components are the transverse electric and magnetic fields E_z and H_y , and the longitudinal field E_x . The circular dipole exploits spin-momentum locking [6,28–31] to achieve $\mathbf{p} \cdot \mathbf{E}^* = p_x E_x^* + p_z E_z^* = 0$ for the mode propagating to the left or right, thereby showing unidirectional excitation in the opposite direction. Analogously, circular magnetic dipoles directionally excite s -polarized modes when $\mathbf{m} \cdot \mu \mathbf{H}^* = 0$.

To describe the nature of the other two sources, however, we must also take into account the relative phase and amplitude between \mathbf{E} and \mathbf{H} . Their relation can be exploited such that the electric and magnetic coupling terms interfere destructively between each other $\mathbf{p} \cdot \mathbf{E}^* + \mathbf{m} \cdot \mu \mathbf{H}^* = 0$. In other words, the mode excited by the electric dipole \mathbf{p} in a given direction is exactly cancelled out by the one excited by the magnetic dipole \mathbf{m} after their superposition. The Huygens source exploits the fixed relative amplitude and phase that exists between the transverse field components E_z and H_y , which depends on the propagation direction of the mode, as dictated by the

Poynting vector. This relation is a well-known property of plane waves that extends directly into evanescent and guided waves.

The Janus dipole exploits the locked amplitude and phase relation that exists between H_y and the longitudinal electric field E_x . The unique feature of the Janus dipole, which distinguishes it from the other two, is that the modes excited by the electric p_x and magnetic m_y dipoles simultaneously interfere destructively for *both* propagation directions. This is possible because the ratio between E_x and H_y is dictated by the reactive power flow vector, and it is independent of the mode's left or right propagation direction (time reversal). This is universally true, at any location, on any waveguide, as follows from the even time-reversal (T) symmetry of the reactive power flow [see Fig. 1(b)]. Thus, a Janus dipole can be designed to achieve polarization and position-dependent “noncoupling” in *every scenario where longitudinal fields are present*, such as *inside* nanowires and photonic crystal waveguides, not being limited to external evanescent coupling as illustrated here. This is a remarkable topological property of near-field polarization in addition to transverse spin [28]. Both the circular and Janus dipole rely on the longitudinal component of the field, while the Huygens source does not. This explains why circular and Janus dipoles are not directional in the far field [4,13], as plane waves have no longitudinal field.

Figure 3 shows the three dipole sources embedded between two waveguides, metal-air interfaces supporting

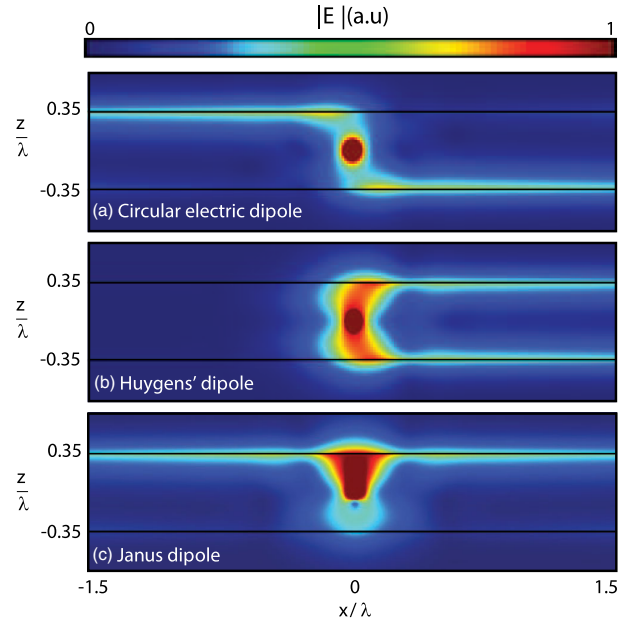


FIG. 3. Amplitude of the electric field generated by (a) a circular dipole, (b) a Huygens antenna, and (c) a Janus dipole embedded in the center of a metal-air-metal waveguide, with $\epsilon = -1.5 + 0.02i$ and $\mu = 1$. The distance between the two waveguides is 0.7λ . These fields have been simulated using Comsol Multiphysics.

surface plasmons as an example, at a distance such that light from the dipole can couple to both waveguides, but with negligible coupling between the waveguides for the propagation distances considered. The circular dipole couples into opposite directions for the waveguides placed above or below the dipole, while the Huygens dipole couples in the same direction for both. Most interestingly, while these two sources exhibit left-right directionality, the Janus dipole exhibits a front-back directionality. While it does not excite the waveguide placed below, it does however excite both directions in the waveguide above it, *regardless of its distance to either*. In this way, the Janus dipole is topologically protected from coupling into the waveguide facing its noncoupling side. This arises because the ratio between E_x and H_y in evanescent waves is independent of the propagation direction but does depend on the *direction of evanescent decay*. This remarkable and inherently broadband behavior suggests novel potential applications in optical nanorouting and signal processing. Importantly, all the directionality properties described in Fig. 3 are robust and independent of the distance of the dipoles to the waveguides. The symmetry of excitations follows directly from that of the sources themselves. A numerical simulation of a Janus dipole between two nanophotonic silicon waveguides is provided in the Supplemental Material (SM) [51].

The design of dipoles exhibiting near-field interference can be done in a general case using Fermi's golden rule, as long as the modal fields are known. However, we now provide a simple complete theory for the specific case of dipoles coupling into *evanescent fields* of planar waveguides, as in Figs. 2 and 3, showing how the three elemental dipoles arise as complete solutions to a single equation. We align our reference system with the propagation direction of the mode, such that the wave vector of the evanescent field is given by $\mathbf{k} = (k_x, k_y, k_z) = (\pm k_m, 0, \pm i\alpha_m)$, where k_m is the propagation constant of the mode, $\alpha_m = (k_m^2 - k^2)^{1/2}$ accounts for the evanescent nature and k is the wave number of the medium. The sign of $\pm k_m$ determines the propagation direction, while the sign of $\pm i\alpha_m$ gives the direction of evanescent decay, which depends on whether the waveguide is below (positive) or above (negative) the dipole. We can write the three field components of p -polarized modes in a vector of the form $\mathbf{F}_p = (E_x, c\mu H_y, E_z)$ and the corresponding dipole moment components as $\mathbf{q}_p = (p_x, m_y/c, p_z)$, so that Fermi's golden rule reduces to a simple scalar product $|\mathbf{q}_p \cdot \mathbf{F}_p^*|^2$. Maxwell's equations demand that p -polarized fields with $k_y = 0$ are always given by $\mathbf{F}_p \propto [(\pm i\alpha_m/k), 1, -(\pm k_m/k)]$ [13,28], irrespective of the nature of the waveguide. The key aspect underpinning all phenomena described in this work is that each pair of these three components has a fixed amplitude and phase relation between them. Indeed, each of the three elemental dipole sources is derived from the relationship between each of the three possible pairs of field

components [Fig. 2(e)]. To obtain near-field interference effects, we solve the equation that achieves zero coupling of the dipoles into a given mode:

$$\mathbf{q}_p \cdot \mathbf{F}_p^* = \left(p_x, \frac{m_y}{c}, p_z \right) \cdot \left(\frac{\pm i\alpha_m}{k}, 1, -\frac{\pm k_m}{k} \right)^* = 0. \quad (2)$$

Mathematically, this simple equation defines a geometric plane of solutions given by the subspace of dipole vectors \mathbf{q}_p , which are orthogonal to \mathbf{F}_p . This unifies all possible ways to achieve directional evanescent coupling of p -polarized modes from electric and magnetic dipole sources, providing a general framework for near-field directionality in planar geometries. Each of the sources discussed above corresponds to intersections of this plane with the p_x , m_y , or $p_z = 0$ planes. Alternatively, each dipole corresponds to the intersection of two planes given by Eq. (2) but for different pairs of sign combinations in k_m and α_m , explaining why each case shows zero excitation of exactly two directions in Fig. 3. A summary of all possible mathematical solutions to this equation is given in Table I. Notice that the dipoles are fine-tuned to achieve a perfect contrast ratio for a specific mode k_m , but the simplest versions, in which $(p_x, m_y/c, p_z) \propto (1, 0, \pm i)$, $(0, \pm 1, 1)$ and $(1, \pm i, 0)$, also work remarkably well as shown in Fig. 2. The optimized Huygens dipole $(\pm k_m^*/k)p = (m/c)$ constitutes a generalized Kerker's condition that works for both propagating and evanescent waves, and reduces to Eq. (1) when $k_m = k$. Each of the three elemental sources is obtainable as a linear superposition of the other two. Finally, we can consider the entire geometric plane of solutions obtained by linear combinations of the elemental sources, resulting in an infinite range of electric and magnetic dipoles that verify Eq. (2).

Similar considerations are valid for s -polarized modes (see SM [51] for details). Solutions are given in Table I. In complete physical analogy to the p -polarized case, the same three elemental dipoles can be derived, but swapping the roles of the electric and magnetic moments. Table I therefore provides all possible solutions for near-field directionality from a dipole source in the general case of

TABLE I. Elemental dipole sources for near-field directionality in planar waveguides. Optimized dipoles use $\hat{k}_m = k_m^*/k$ and $\hat{\alpha}_m = \alpha_m^*/k$, while the simplest dipoles use $\hat{\alpha}_m, \hat{k}_m \approx 1$. In the general solution, $\mathbf{q}_{p/s}^i$ and $\mathbf{q}_{p/s}^j$ stand for any two of the three elemental dipoles with arbitrary complex coefficients a and b .

| | p -polarization $\mathbf{q}_p = (p_x, m_y/c, p_z)$ | s -polarization $\mathbf{q}_s = (m_x/c, p_y, m_z/c)$ |
|------------|---|---|
| Elliptical | $(\pm \hat{k}_m, 0, \mp i\hat{\alpha}_m)$ | $(\pm \hat{k}_m, 0, \mp i\hat{\alpha}_m)$ |
| Huygens | $(0, \pm \hat{k}_m, 1)$ | $(0, \pm \hat{k}_m, -1)$ |
| Janus | $(1, \pm i\hat{\alpha}_m, 0)$ | $(-1, \pm i\hat{\alpha}_m, 0)$ |
| General | $\mathbf{q}_p = a\mathbf{q}_p^i + b\mathbf{q}_p^j$ | $\mathbf{q}_s = a\mathbf{q}_s^i + b\mathbf{q}_s^j$ |

planar geometries, but we would like to emphasize that following a spectral interpretation [52] (see SM [51]), all dipoles derived in Table I are excellent approximations to their optimum when placed near arbitrary waveguides, as was shown in Ref. [13].

In conclusion, previous approaches to guided optics directionality from dipolar sources made use of the spin of the guided mode's fields \mathbf{E} and \mathbf{H} , neglecting their mutual amplitude and phase relations. By considering the complete vector structure of electromagnetic fields, we provide a unified theory describing all possible dipole sources exhibiting far- and near-field directionality with planar structures; these considerations can be applied to arbitrary geometries once the modes supported by the waveguide are known. The implementation of these new sources using resonant plasmonic or dielectric nanoparticles and their integration in photonic circuitry will provide a step change in the already broad range of near-field directionality applications, currently based on circular dipoles exclusively. We expect novel ideas to emerge in quantum optics, photonic nanorouting, photonic logical circuits, optical forces and torques of particles in near-field environments, inverse and reciprocal scenarios for polarization synthesis, integrated polarimeters, and other unforeseen devices throughout the whole electromagnetic spectrum.

This work was supported by European Research Council Starting Grant ERC-2016-STG-714151-PSINFONI and EPSRC (UK). A.Z. acknowledges support from the Royal Society and the Wolfson Foundation. The authors wish to thank K. Y. Bliokh for helpful discussions.

* michela.picardi@kcl.ac.uk

- [1] Editorial: Not so small, *Nat. Photonics* **8**, 877 (2014).
- [2] N. Yu and F. Capasso, Flat optics with designer metasurfaces, *Nat. Mater.* **13**, 139 (2014).
- [3] D.E. Chang, V. Vuletić, and M.D. Lukin, Quantum nonlinear optics photon by photon, *Nat. Photonics* **8**, 685 (2014).
- [4] F. J. Rodríguez-Fortuño, G. Marino, P. Ginzburg, D. O'Connor, A. Martínez, G. A. Wurtz, and A. V. Zayats, Near-field interference for the unidirectional excitation of electromagnetic guided modes, *Science* **340**, 328 (2013).
- [5] P. V. Kapitanova, P. Ginzburg, F. J. Rodríguez-Fortuño, D. S. Filonov, P. M. Voroshilov, P. A. Belov, A. N. Poddubny, Y. S. Kivshar, G. A. Wurtz, and A. V. Zayats, Photonic spin Hall effect in hyperbolic metamaterials for polarization-controlled routing of subwavelength modes, *Nat. Commun.* **5**, 3226 (2014).
- [6] A. Aiello, P. Banzer, M. Neugebauer, and G. Leuchs, From transverse angular momentum to photonic wheels, *Nat. Photonics* **9**, 789 (2015).
- [7] A. Espinosa-Soria and A. Martínez, Transverse spin and spin-orbit coupling in silicon waveguides, *IEEE Photonics Technol. Lett.* **28**, 1561 (2016).
- [8] R. J. Coles, D. M. Price, J. E. Dixon, B. Royall, E. Clarke, P. Kok, M. S. Skolnick, A. M. Fox, and M. N. Makhonin, Chirality of nanophotonic waveguide with embedded quantum emitter for unidirectional spin transfer, *Nat. Commun.* **7**, 11183 (2016).
- [9] B. le Feber, N. Rotenberg, and L. Kuipers, Nanophotonic control of circular dipole emission, *Nat. Commun.* **6**, 6695 (2015).
- [10] A. A. Zharov and N. A. Zharova, Control of surface plasmon excitation via the scattering of light by a nanoparticle, *J. Exp. Theor. Phys.* **123**, 17 (2016).
- [11] Y.-H. Wang, R.-C. Jin, J.-Q. Li, F. Zhong, H. Liu, I. Kim, Y. Jo, J. Rho, and Z.-G. Dong, Photonic spin-Hall effect by the spin-orbit interaction in a metasurface with elliptical nanostructures, *Appl. Phys. Lett.* **110**, 101908 (2017).
- [12] D. Garoli, P. Zilio, F. De Angelis, and Y. Gorodetski, Helicity locking of chiral light emitted from a plasmonic nanotaper, *Nanoscale* **9**, 6965 (2017).
- [13] M. F. Picardi, A. Manjavacas, A. V. Zayats, and F. J. Rodríguez-Fortuño, Unidirectional evanescent-wave coupling from circularly polarized electric and magnetic dipoles: An angular spectrum approach, *Phys. Rev. B* **95**, 245416 (2017).
- [14] L. Marrucci, Quantum optics: Spin gives direction, *Nat. Phys.* **11**, 9 (2015).
- [15] I. J. Luxmoore, N. A. Wasley, A. J. Ramsay, A. C. T. Thijssen, R. Oulton, M. Hugues, S. Kasture, V. G. Achanta, A. M. Fox, and M. S. Skolnick, Interfacing Spins in an InGaAs Quantum Dot to a Semiconductor Waveguide Circuit Using Emitted Photons, *Phys. Rev. Lett.* **110**, 037402 (2013).
- [16] R. Mitsch, C. Sayrin, B. Albrecht, P. Schneeweiss, and A. Rauschenbeutel, Quantum state-controlled directional spontaneous emission of photons into a nanophotonic waveguide, *Nat. Commun.* **5**, 5713 (2014).
- [17] J. Petersen, J. Volz, and A. Rauschenbeutel, Chiral nanophotonic waveguide interface based on spin-orbit interaction of light, *Science* **346**, 67 (2014).
- [18] M. Neugebauer, T. Bauer, P. Banzer, and G. Leuchs, Polarization tailored light driven directional optical nanobeacon, *Nano Lett.* **14**, 2546 (2014).
- [19] A. Espinosa-Soria, F. J. Rodríguez-Fortuño, A. Griol, and A. Martínez, On-chip optimal stokes nanopolarimetry based on spin-orbit interaction of light, *Nano Lett.* **17**, 3139 (2017).
- [20] D. O'Connor, P. Ginzburg, F. J. Rodríguez-Fortuño, G. A. Wurtz, and A. V. Zayats, Spinorbit coupling in surface plasmon scattering by nanostructures, *Nat. Commun.* **5**, 5327 (2014).
- [21] F. J. Rodríguez-Fortuño, D. Puerto, A. Griol, L. Bellieres, J. Martí, and A. Martínez, Universal method for the synthesis of arbitrary polarization states radiated by a nanoantenna, *Laser Photonics Rev.* **8**, L27 (2014).
- [22] F. J. Rodríguez-Fortuño, I. Barber-Sanz, D. Puerto, A. Griol, and A. Martínez, Resolving light handedness with an on-chip silicon microdisk, *ACS Photonics* **1**, 762 (2014).
- [23] F. J. Rodríguez-Fortuño, D. Puerto, A. Griol, L. Bellieres, J. Martí, and A. Martínez, Sorting linearly polarized photons with a single scatterer, *Opt. Lett.* **39**, 1394 (2014).
- [24] C. Sayrin, C. Junge, R. Mitsch, B. Albrecht, D. O'Shea, P. Schneeweiss, J. Volz, and A. Rauschenbeutel, Nanophotonic

- Optical Isolator Controlled by the Internal State of Cold Atoms, *Phys. Rev. X* **5**, 041036 (2015).
- [25] J. Ma, X. Xi, Z. Yu, and X. Sun, Hybrid graphene/silicon integrated optical isolators with photonic spin-orbit interaction, *Appl. Phys. Lett.* **108**, 151103 (2016).
- [26] K. Y. Bliokh and F. Nori, Transverse and longitudinal angular momenta of light, *Phys. Rep.* **592**, 1 (2015).
- [27] K. Y. Bliokh, F. J. Rodríguez-Fortuño, F. Nori, and A. V. Zayats, Spin-orbit interactions of light, *Nat. Photonics* **9**, 796 (2015).
- [28] K. Y. Bliokh, D. Smirnova, and F. Nori, Quantum spin Hall effect of light, *Science* **348**, 1448 (2015).
- [29] C. Junge, D. O'Shea, J. Volz, and A. Rauschenbeutel, Strong Coupling Between Single Atoms and Nontransversal Photons, *Phys. Rev. Lett.* **110**, 213604 (2013).
- [30] K. Y. Bliokh, A. Y. Bekshaev, and F. Nori, Extraordinary momentum and spin in evanescent waves, *Nat. Commun.* **5**, 3300 (2014).
- [31] T. Van Mechelen and Z. Jacob, Universal spin-momentum locking of evanescent waves, *Optica* **3**, 118 (2016).
- [32] I. S. Sinev, A. A. Bogdanov, F. E. Komissarenko, K. S. Frizyuk, M. I. Petrov, I. S. Mukhin, S. V. Makarov, A. K. Samusev, A. V. Lavrinenko, and I. V. Iorsh, Chirality driven by magnetic dipole response for demultiplexing of surface waves, *Laser Photonics Rev.* **11**, 1700168 (2017).
- [33] S.-Y. Lee, I.-M. Lee, J. Park, S. Oh, W. Lee, K.-Y. Kim, and B. Lee, Role of Magnetic Induction Currents in Nanoslit Excitation of Surface Plasmon Polaritons, *Phys. Rev. Lett.* **108**, 213907 (2012).
- [34] A. B. Evlyukhin and S. I. Bozhevolnyi, Resonant unidirectional and elastic scattering of surface plasmon polaritons by high refractive index dielectric nanoparticles, *Phys. Rev. B* **92**, 245419 (2015).
- [35] M. Neugebauer, P. Woźniak, A. Bag, G. Leuchs, and P. Banzer, Polarization-controlled directional scattering for nanoscopic position sensing, *Nat. Commun.* **7**, 11286 (2016).
- [36] M. Kerker, D.-S. Wang, and C. L. Giles, Electromagnetic scattering by magnetic spheres, *J. Opt. Soc. Am.* **73**, 765 (1983).
- [37] X. Zambrana-Puyalto, I. Fernandez-Corbaton, M. L. Juan, X. Vidal, and G. Molina-Terriza, Duality symmetry and kerker conditions, *Opt. Lett.* **38**, 1857 (2013).
- [38] A. B. Evlyukhin, S. M. Novikov, U. Zywietz, R. L. Eriksen, C. Reinhardt, S. I. Bozhevolnyi, and B. N. Chichkov, Demonstration of magnetic dipole resonances of dielectric nanospheres in the visible region, *Nano Lett.* **12**, 3749 (2012).
- [39] Y. H. Fu, A. I. Kuznetsov, A. E. Miroshnichenko, Y. F. Yu, and B. Lukyanchuk, Directional visible light scattering by silicon nanoparticles, *Nat. Commun.* **4**, 1527 (2013).
- [40] D. Permyakov, I. Sinev, D. Markovich, P. Ginzburg, A. Samusev, P. Belov, V. Valuckas, A. I. Kuznetsov, B. S. Luk'yanchuk, A. E. Miroshnichenko, D. N. Neshev, and Y. S. Kivshar, Probing magnetic and electric optical responses of silicon nanoparticles, *Appl. Phys. Lett.* **106**, 171110 (2015).
- [41] A. I. Kuznetsov, A. E. Miroshnichenko, M. L. Brongersma, Y. S. Kivshar, and B. Lukyanchuk, Optically resonant dielectric nanostructures, *Science* **354**, aag2472 (2016).
- [42] J. M. Geffrin, B. García-Cámara, R. Gómez-Medina, P. Albella, L. S. Froufe-Pérez, C. Eyraud, A. Litman, R. Vaillon, F. González, M. Nieto-Vesperinas, J. J. Sáenz, and F. Moreno, Magnetic and electric coherence in forward-and back-scattered electromagnetic waves by a single dielectric subwavelength sphere, *Nat. Commun.* **3**, 1171 (2012).
- [43] S. Person, M. Jain, Z. Lapin, J. J. Sáenz, G. Wicks, and L. Novotny, Demonstration of zero optical backscattering from single nanoparticles, *Nano Lett.* **13**, 1806 (2013).
- [44] I. Staude, A. E. Miroshnichenko, M. Decker, N. T. Fofang, S. Liu, E. Gonzales, J. Dominguez, T. S. Luk, D. N. Neshev, I. Brener, and Y. Kivshar, Tailoring directional scattering through magnetic and electric resonances in subwavelength silicon nanodisks, *ACS Nano* **7**, 7824 (2013).
- [45] M. Nieto-Vesperinas, R. Gomez-Medina, and J. J. Saenz, Angle-suppressed scattering and optical forces on submicrometer dielectric particles, *J. Opt. Soc. Am. A* **28**, 54 (2011).
- [46] T. Coenen, F. B. Arango, A. F. Koenderink, and A. Polman, Directional emission from a single plasmonic scatterer, *Nat. Commun.* **5**, 3250 (2014).
- [47] L. Wei, N. Bhattacharya, and H. P. Urbach, Adding a spin to kerkers condition: Angular tuning of directional scattering with designed excitation, *Opt. Lett.* **42**, 1776 (2017).
- [48] R. Paniagua-Domínguez, Y. F. Yu, A. E. Miroshnichenko, L. A. Krivitsky, Y. H. Fu, V. Valuckas, L. Gonzaga, Y. T. Toh, A. Y. S. Kay, B. Lukyanchuk, and A. I. Kuznetsov, Generalized Brewster effect in dielectric metasurfaces, *Nat. Commun.* **7**, 10362 (2016).
- [49] K. Y. Bliokh, A. Y. Bekshaev, and F. Nori, Optical Momentum, Spin, and Angular Momentum in Dispersive Media, *Phys. Rev. Lett.* **119**, 073901 (2017).
- [50] K. Y. Bliokh, Y. S. Kivshar, and F. Nori, Magnetoelectric Effects in Local Light-Matter Interactions, *Phys. Rev. Lett.* **113**, 033601 (2014).
- [51] See Supplemental Material at <http://link.aps.org/supplemental/10.1103/PhysRevLett.120.117402> for a numerical simulation of a Janus dipole between 3D silicon waveguides; and the description of *s*-polarized evanescent fields; and the angular spectrum approach.
- [52] M. C. Teich and B. Saleh, *Fundamentals of Photonics* (Wiley Interscience, New York, 1991).